Supporting Information

Two-Dimensional Confined Electron Donor–Acceptor Co-intercalated Inorganic/Organic Nanocomposites: An Effective Photocatalyst for Dye Degradation

Shufang Zheng,[†] Jun Lu,*[,†,‡], Jingjing Shi,[†] and Xue Duan[†]

[†]State Key Laboratory of Chemical Resource Engineering, Beijing University of Chemical Technology, 15 Beisanhuan East Road, P. Box 98, Beijing 100029, P. R. China

[‡]Beijing Engineering Center for Hierarchical Catalysts, Beijing University of Chemical Technology, 15 Beisanhuan East Road, P. Box 98, Beijing 100029, P. R. China

List of Contents

Figure S7. XRD patterns of the CuPcTS-PTCB(*x*%)/LDHs composites before and after 10 cycles photodegradation of MO.

2. The photocatalytic degradation of organic dyes for CuPcTS-PTCB(*x*%)/LDHs

Figure S8. The comparison of photodegradation of MO under the simulated solar irradiation.

Figure S9. Photocatalytic degradation of MO, AO, AY, MB, MV and RhB for CuPcTS-PTCB(*x*%)/LDHs.

Figure S10. Photocatalytic activity of (a) CuPcTS/LDHs, (b) PTCB/LDHs, and (c) P25 particles for MO.

Figure S11. Photocatalytic degradation of phenol for CuPcTS-PTCB(49.75%)/LDHs.

Figure S12. Adsorption amounts of MO on CuPcTS-PTCB(*x*%)/LDHs (x = 0, 36.63, 49.75, 63.64, 77.32, 90.91, 100).

Table S2 The BET surface of CuPcTS-PTCB(*x*%)/LDHs (x = 0, 36.63, 49.75, 63.64, 77.32, 90.91, 100)

3. Cyclic voltammograms curves and analysis of energy levels

Figure S13. Cyclic voltammograms curves of Ferrocene.

Figure S14. Cyclic voltammograms curves of CuPcTS, PTCB, CuPcTS/LDHs, and PTCB/LDHs.

Figure S15. Cyclic voltammograms curves of MO, AO, AY, MB, MV, and RhB.

Figure S16. The Current–Voltage curves of CuPcTS-PTCB(49.75%)/LDHs in dark and light at a scanning rate of 50 mV s^{-1}. Inset: the EIS curve of CuPcTS-PTCB(49.75%)/LDHs.

1. Structural characterization and optical absorption spectra of CuPcTS-PTCB(x%)/LDHs

Table S1. The elemental composition of CuPcTS-PTCB(x%)/LDHs

Nominal (x%)	**Chemical Composition**	**Zn/Al Ratio**	**Determined (x%)**
0	$Zn_{0.585}Al_{0.415}(OH)_2\ (C_{32}H_{12}N_8CuO_{12}S_4)_{0.073}\ (OH)_{0.123}\ 3.316H_2O$	1.41	0.00
10	$Zn_{0.595}Al_{0.405}(OH)_2(C_{24}H_8O_8)_{0.037}(C_{32}H_{12}N_8CuO_{12}S_4)_{0.064}\ 2.197H_2O$	1.47	36.63
30	$Zn_{0.603}Al_{0.397}(OH)_2(C_{24}H_8O_8)_{0.049}(C_{32}H_{12}N_8CuO_{12}S_4)_{0.050}\cdot 1.741H_2O$	1.52	49.75
50	$Zn_{0.605}Al_{0.395}(OH)_2(C_{24}H_8O_8)_{0.063}(C_{32}H_{12}N_8CuO_{12}S_4)_{0.036}\cdot 1.873H_2O$	1.53	63.64
70	$Zn_{0.611}Al_{0.389}(OH)_2(C_{24}H_8O_8)_{0.075}(C_{32}H_{12}N_8CuO_{12}S_4)_{0.022}\cdot 1.718H_2O$	1.57	77.32
90	$Zn_{0.606}Al_{0.394}(OH)_2(C_{24}H_8O_8)_{0.090}(C_{32}H_{12}N_8CuO_{12}S_4)_{0.009}\ 2.313H_2O$	1.54	90.91
100	$Zn_{0.595}Al_{0.405}(OH)_2(C_{24}H_8O_8)_{0.101}\ 0.507H_2O$	1.47	100.00

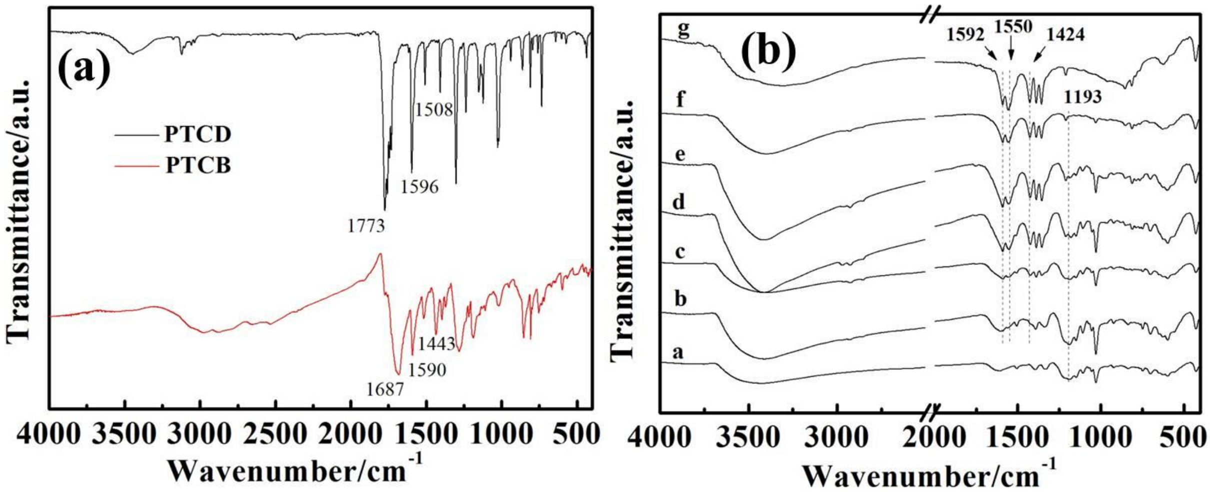

Figure S1 The FT-IR spectra, (a) PTCD and PTCB, (b) a-CuPcTS/LDHs; b-CuPcTS-PTCB(36.63%)/LDHs; c-CuPcTS-PTCB(49.75%)/LDHs; d-CuPcTS-PTCB(63.64%)/LDHs; e-CuPcTS-PTCB(77.73%)/LDHs; f-CuPcTS-PTCB(90.91%)/LDHs; g-PTCB/LDHs.

For the FT-IR spectrum of pristine PTCD (**Figure S1a**), the strong band at 1773 cm^{-1} was the characteristic CO–O–CO stretching vibration of the anhydride, and the bands at 1596 cm^{-1} and 1508 cm^{-1} were due to the skeleton vibration of phenyl ring. When the PTCD was hydrolyzed into PTCB, two bands corresponding to the vibrations of C=O in the –COOH group could be observed at 1687 cm^{-1} and 1590 cm^{-1} (**Figure S1a)**, and the in plane deformation vibration of O–H appeared at 1433 cm^{-1}.[1] For the CuPcTS-PTCB(x%)/LDHs that included PTCB, the bands at 1550 cm^{-1} and 1424 cm^{-1}

were due to the antisymmetric and symmetric stretching vibration of C–O^{-} in the –COO^{-} group. The skeleton vibration of the phenyl ring also appeared at 1592 cm^{-1}. All those indicated that the PTCB was intercalated into $Zn_{1.5}$Al-LDHs. The appearance of the characteristic absorption peak of $-SO_3^{-1}$ at 1193 cm^{-1} (**Figure S1b**) suggested the successful intercalation of CuPcTS into the $Zn_{1.5}$Al-LDHs.[2]

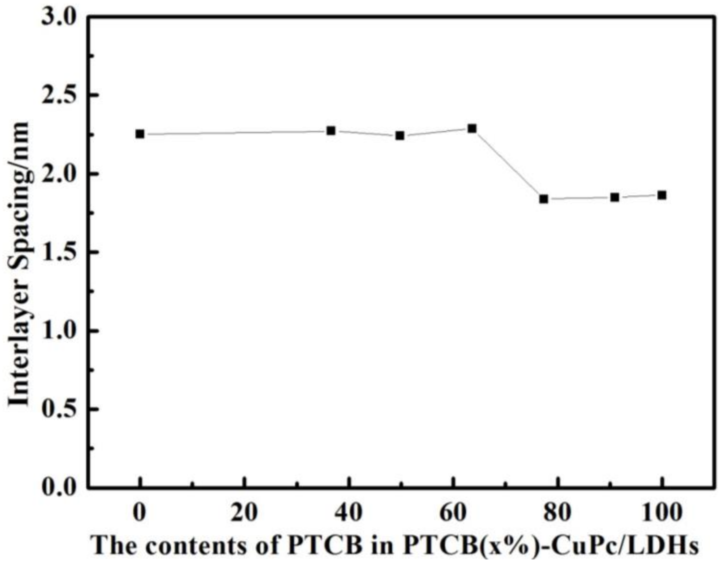

Figure S2. The layer spacing of CuPcTS-PTCB(x%)/LDHs.

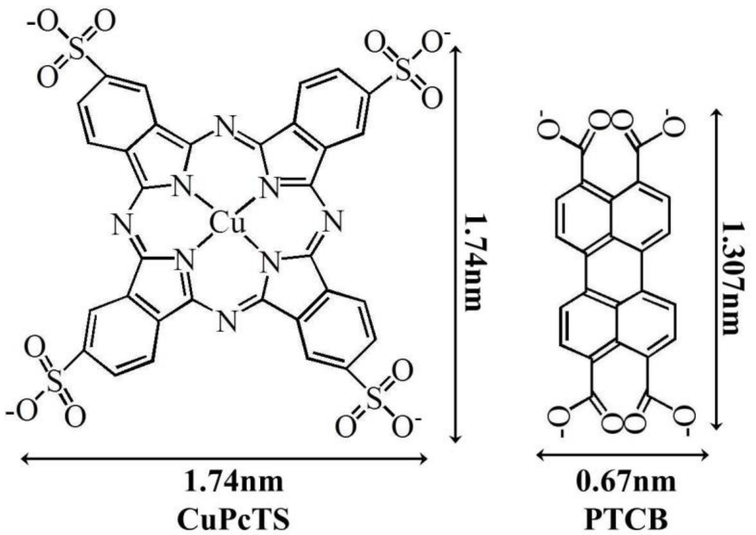

Figure S3. The molecular models of CuPcTS and PTCB calculated by Gaussian 09 software.

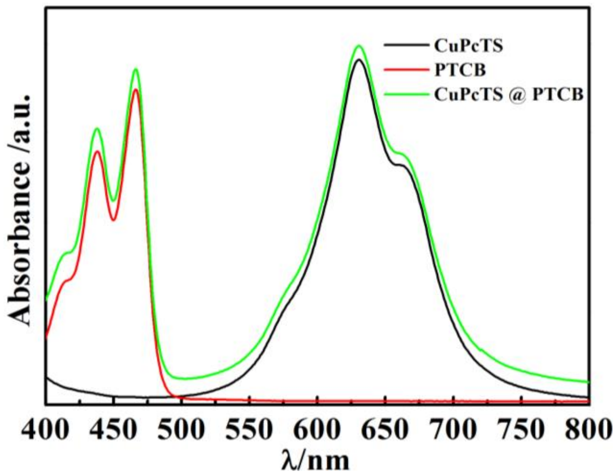

Figure S4. The UV-vis absorption spectra of CuPcTS (15 μmol/L), PTCB (15 μmol/L) and CuPcTS@PTCB (15 μmol/L) aqueous solutions.

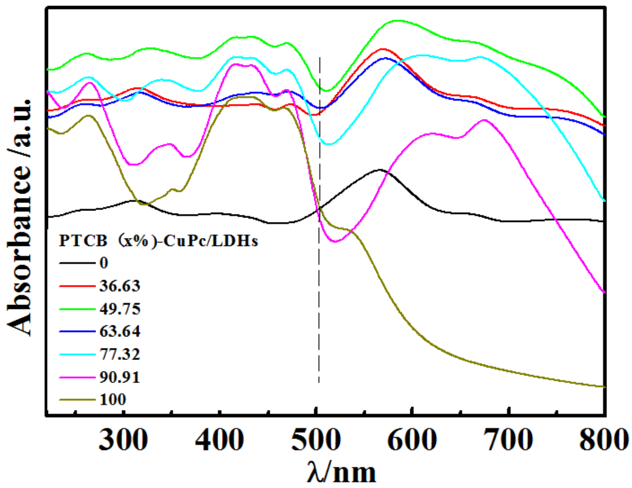

Figure S5. The UV-vis absorption spectra of CuPcTS-PTCB(*x*%)/LDHs.

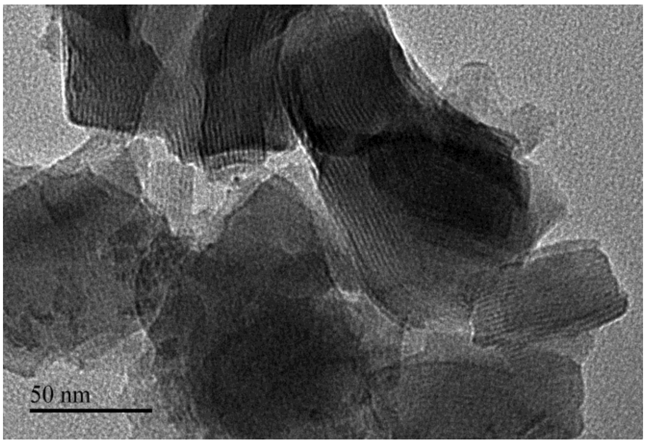

Figure S6. HRTEM image of CuPcTS-PTCB(49.75%)/LDHs after 10 consecutive cycles of catalytic photodegradation of MO.

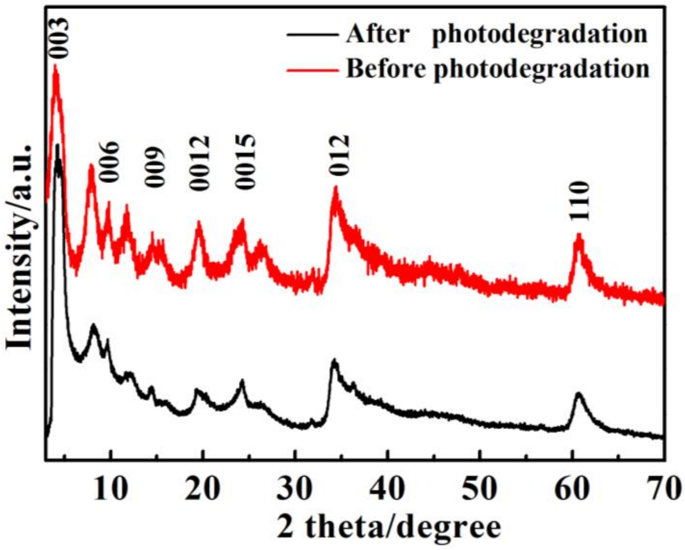

Figure S7. XRD patterns of the CuPcTS-PTCB(x%)/LDHs composites before and after 10 cycles photodegradation of MO.

2. The photocatalytic degradation of organic dyes for CuPcTS-PTCB(x%)/LDHs

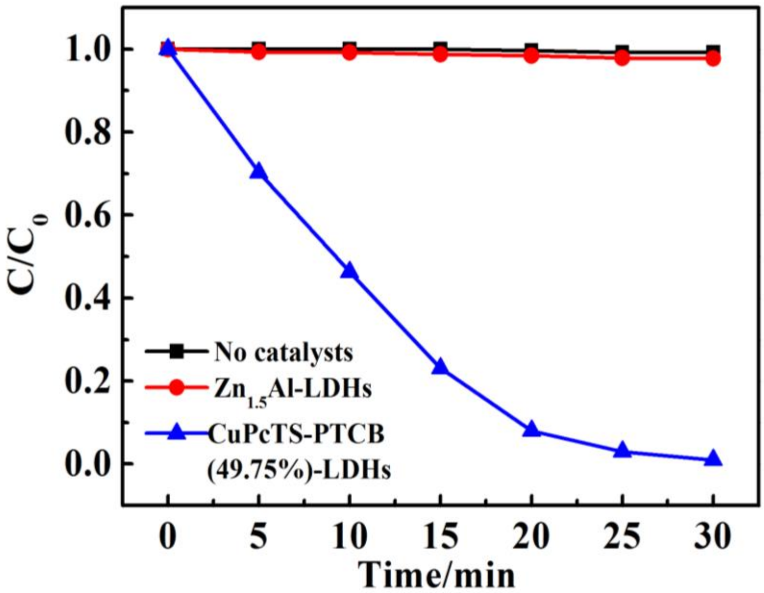

Figure S8. The comparison of photodegradation of MO under the simulated solar irradiation.

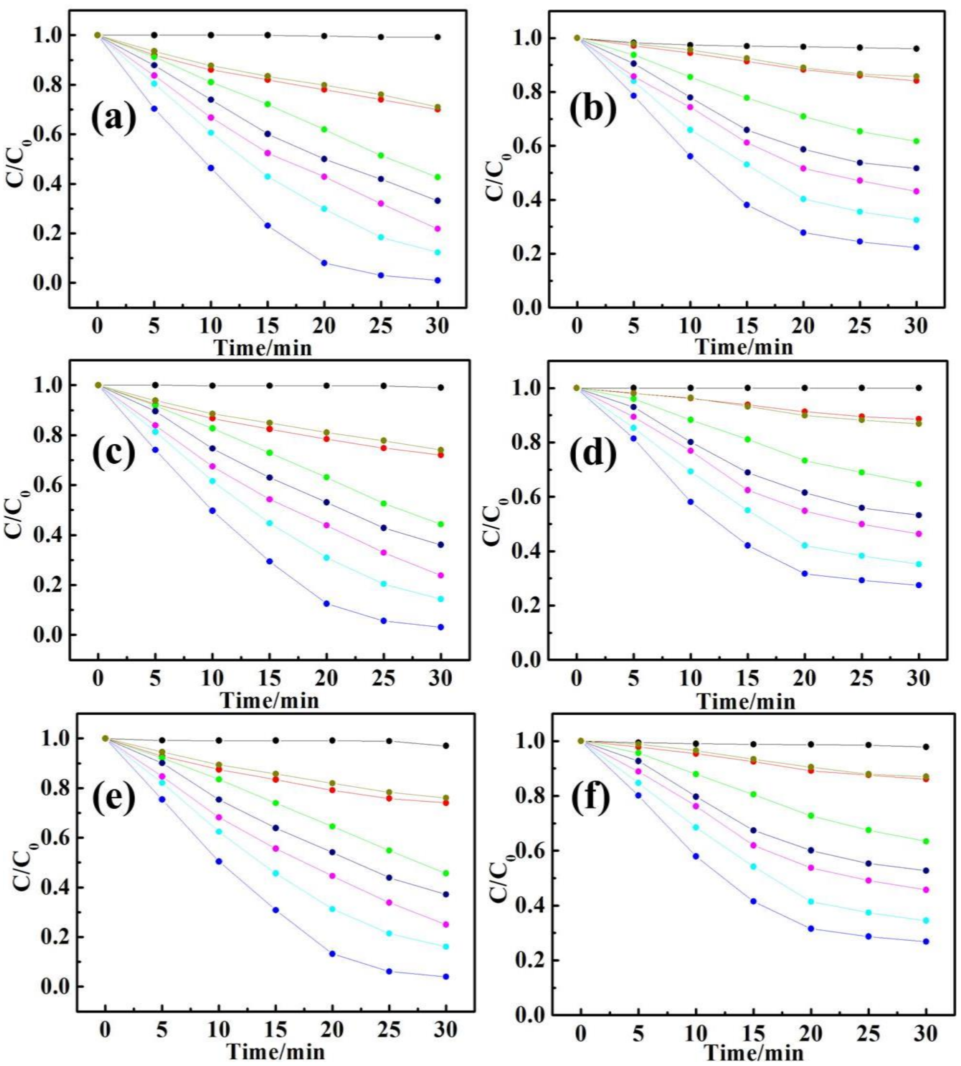

Figure S9. Photocatalytic degradation of MO (a), AO (c), AY (e), MB (b), MV (d) and RhB (f) for CuPcTS-PTCB(*x*%)/LDHs (no catalysts-black, CuPcTS/LDHs-red, CuPcTS-PTCB(36.63%)/LDHs-green, CuPcTS-PTCB(49.75%)/LDHs-blue, CuPcTS-PTCB(63.64%)/LDHs-cyan, CuPcTS-PTCB(77.32%)/LDHs-magenta, CuPcTS-PTCB(90.91%)/LDHs-navy, PTCB/LDHs-dark yellow).

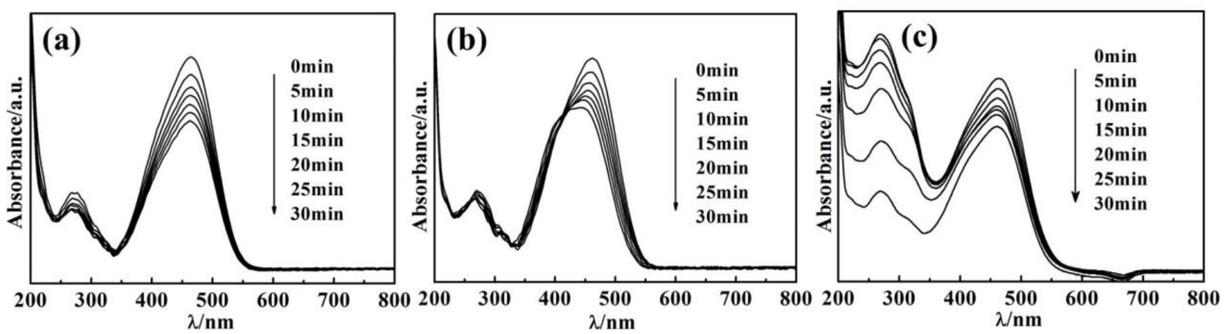

Figure S10. Photocatalytic activity of (a) CuPcTS/LDHs, (b) PTCB/LDHs, and (c) P25 particles for MO.

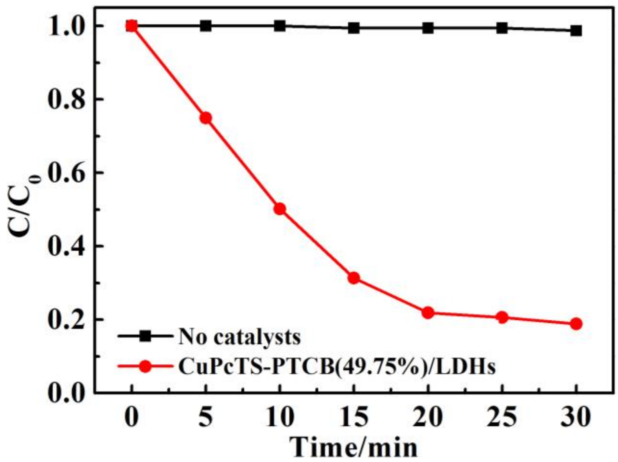

Figure S11. Photocatalytic degradation of phenol for CuPcTS-PTCB(49.75%)/LDHs.

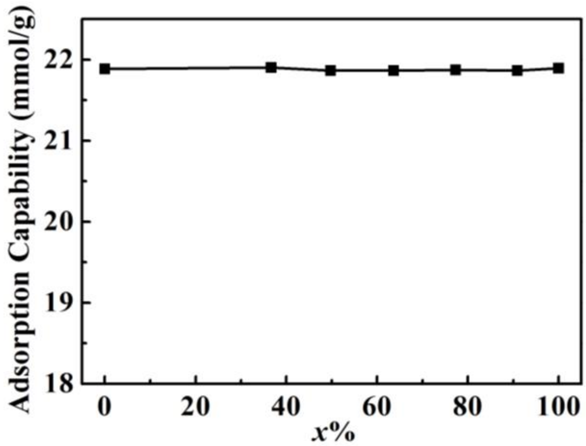

Figure S12. Adsorption amounts of MO on CuPcTS-PTCB(*x*%)/LDHs (*x* = 0, 36.63, 49.75, 63.64, 77.32, 90.91, 100).

Table S2. The BET surface of CuPcTS-PTCB(*x*%)/LDHs (*x* = 0, 36.63, 49.75, 63.64, 77.32, 90.91, 100)

Photocatalyst	BET specific surface area (m^2 g^{-1})
CuPcTS/LDHs	60.83
CuPcTS-PTCB(36.63%)/LDHs	61.24
CuPcTS-PTCB(49.75%)/LDHs	52.82
CuPcTS-PTCB(63.64%)/LDHs	62.92
CuPcTS-PTCB(77.32%)/LDHs	53.14
CuPcTS-PTCB(90.91%)/LDHs	64.46
PTCB/LDHs	66.61

3. Cyclic voltammograms curves and analysis of energy levels

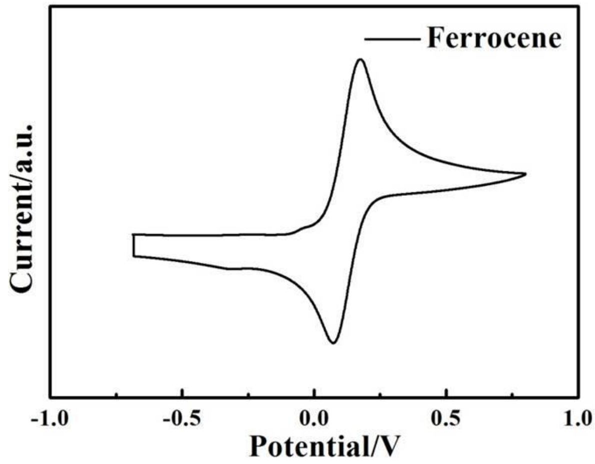

Figure S13. Cyclic voltammograms curves of Ferrocene.

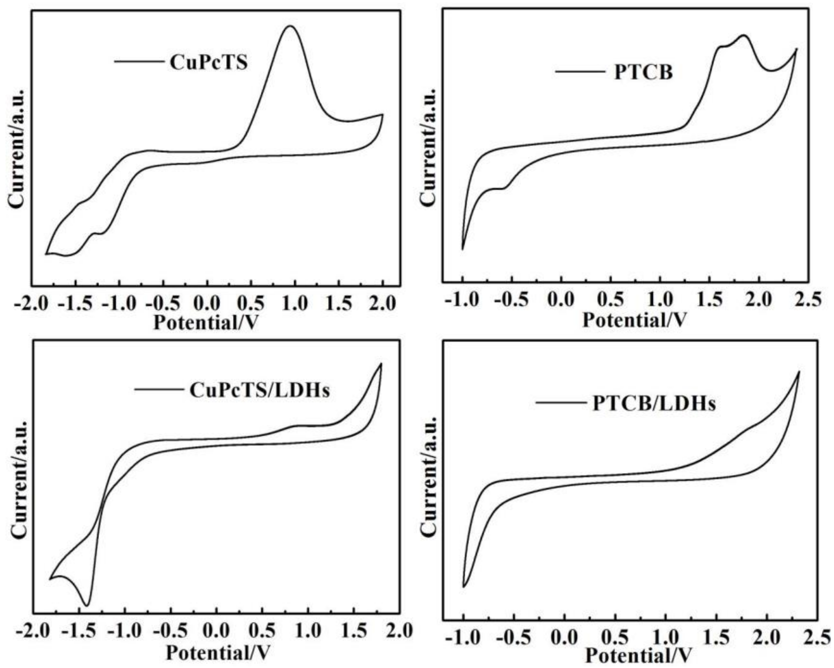

Figure S14. Cyclic voltammograms curves of CuPcTS, PTCB, CuPcTS/LDHs, and PTCB/LDHs. The CV curves of CuPcTS/LDHs and PTCB/LDHs single-intercalated samples were also measured, provided that no remarkable difference in energy levels between the co-intercalated and single-intercalated composites.

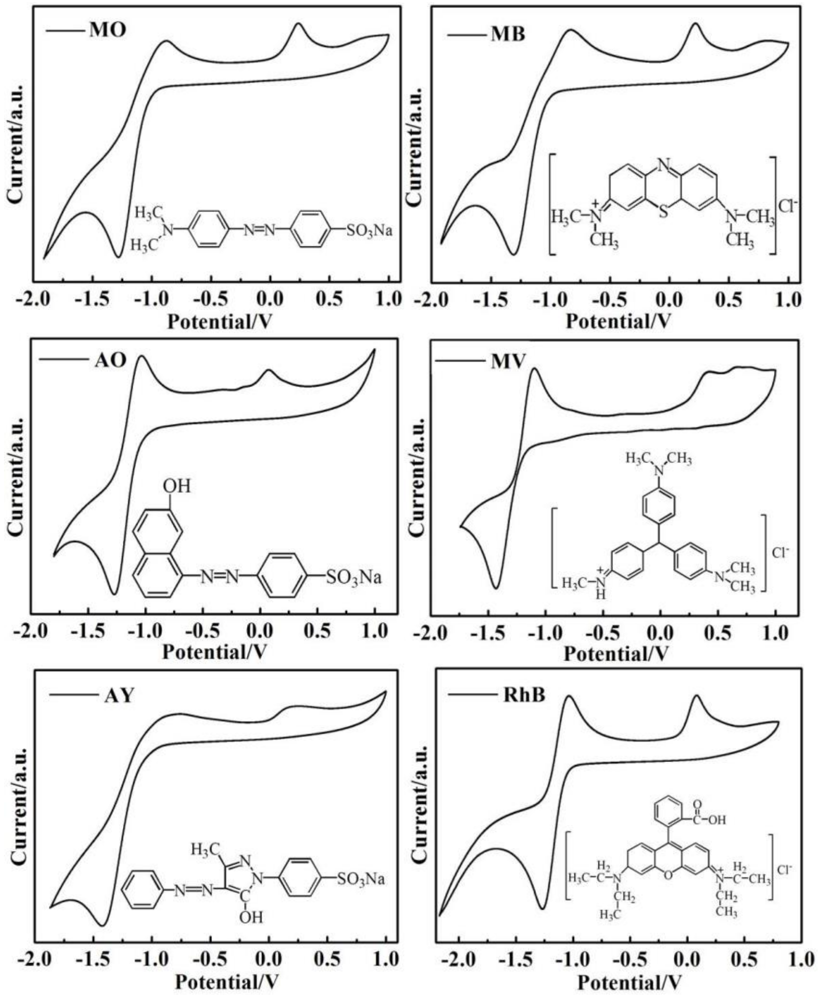

Figure S15. Cyclic voltammograms curves of MO, AO, AY, MB, MV, and RhB.

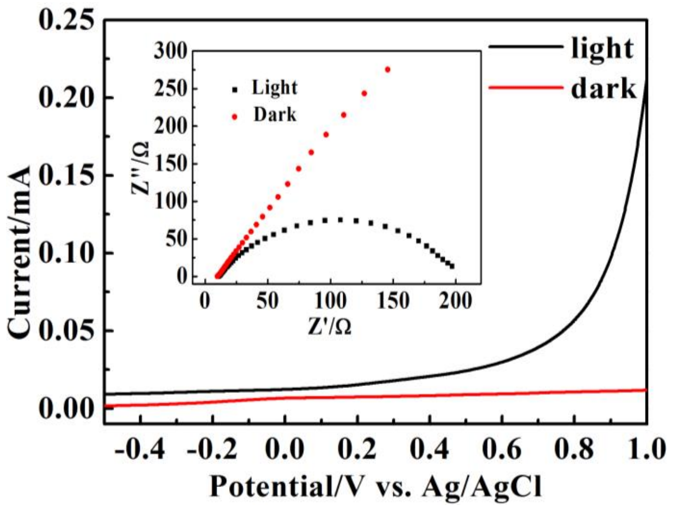

Figure S16. The Current–Voltage curves of CuPcTS-PTCB(49.75%)/LDHs in dark and light at a scanning rate of 50 mV s $^{-1}$. Inset: the EIS curve of CuPcTS-PTCB(49.75%)/LDHs.

References

[1] D. Yan, J. Lu, M. Wei, J. Ma, D. G. Evans and X. Duan, *Phy. Chem. Chem. Phy.*, 2009, **11**, 9200–9209.

[2] J. Wang, M. Wei, G. Rao, D. G. Evans and X. Duan, *J. Solid State Chem.*, 2004, **177**, 366–371.